Interaction between Succinic Acid and Sulfuric Acid-Base Clusters

Yun Lin,[1] Yuemeng Ji,[1,2,*] Yixin Li,[1] Jeremiah Secrest,[1] Wen Xu,[3] Fei Xu,[4] Yuan Wang,[5] Taicheng An,[2] and Renyi Zhang[1,*]

[1]Department of Atmospheric Sciences and Department of Chemistry, Texas A&M University, College Station, TX 77843, USA

[2]Institute of Environmental Health and Pollution Control, Guangdong University of Technology, Guangzhou 510006, China

[3]Aerodyne Research Inc, Billerica, MA 01821, USA

[4]School of Environmental Science and Engineering, Shandong University, Jinan 250100, China

[5]Division of Geological and Planetary Sciences, California Institute of Technology, Pasadena, CA, 91125, USA

* Corresponding authors: Renyi Zhang, renyi-zhang@tamu.edu; Yuemeng Ji, jiym99@163.com

ABSTRACT. Dicarboxylic acids likely participate in the formation of pre-nucleation clusters to facilitate new particle formation in the atmosphere, but the detailed mechanism leading to the formation of multi-component critical nucleus involving organic acids, sulfuric acid (SA), base species, and water remains unclear. In this study, theoretical calculations are performed to elucidate the interactions between succinic acid (SUA) and clusters consisting of SA-ammonia (AM)/dimethylamine (DMA) in the presence of hydration of up to six water molecules. Formation of the hydrated SUA•SA•base clusters is energetically favorable, triggering proton transfer from SA to the base molecule to form new covalent bonds or strengthening the pre-existing covalent bonds. The presence of SUA promotes hydration of the SA•AM and SA•AM•DMA clusters but dehydration of the SA•DMA clusters. At equilibrium, SUA competes with the second SA molecule for addition to the SA•base clusters at atmospherically relevant concentrations. The clusters containing both the base and organic acid are capable of further binding with acid molecules to promote subsequent growth. Our results indicate that the multi-component nucleation involving organic acids, sulfuric acid, and base species promotes new particle formation in the atmosphere, particularly under polluted conditions with high concentration of diverse organic acids.

1. INTRODUCTION

Atmospheric aerosols are important to several issues, including climate, visibility and human health (IPCC, 2013; Zhang et al., 2015). In particular, aerosols influence the Earth energy budget directly by absorbing/scattering incoming solar radiation and indirectly by acting as cloud condensation nuclei (CCN)/ice nuclei (IN), which impact the lifetime, coverage, precipitation efficiency, and albedo of clouds (Andreae et al., 2004; Fan et al., 2007; Li et al., 2008). Currently, the indirect radiative forcing of aerosols represents the largest uncertainty in climate predictions (IPCC, 2013). In addition, ultrafine aerosols likely exert important impacts on adverse human health outcomes (Rychlik et al., 2019). New particle formation (NPF) has been observed under diverse environmental conditions (Kulmala and Kerminen, 2008; Zhang et al., 2012; Wang et al., 2013; Guo et al., 2014; Bianchi et al., 2016; Wang et al., 2016) and contributes up to half of the CCN population in the troposphere (Merikanto et al., 2009; Yue et al., 2011). NPF involves two distinct steps, i.e., nucleation to form a critical nucleus and subsequent growth of newly formed nanoparticles to a larger size (> 3 nm). Currently, the identities and the roles of chemical species involved in NPF are not fully understood at the molecular level, hindering the development of physically-based parameterization to include NPF in atmospheric models (Zhang et al. 2010; Cai and Jiang, 2017). Sulfuric acid (SA) is believed to be the most common atmospheric nucleation species, and ammonia (AM)/amines further stabilize the hydrated sulfuric acid clusters and enhance the nucleation (Kuang et al, 2010; Yue et al., 2010; Erupe et al., 2011; Yu et al., 2012; Qiu et al., 2013; Wang et al., 2018; Yao et al., 2018). However, neither the sulfuric acid-water binary nucleation nor ammonia/amine-containing ternary nucleation sufficiently explains the measured NPF rates in the lower troposphere (Xu et al., 2010a; Zhang et al. 2012), suggesting

53 the role of other chemical species, such as organic acids, in NPF (Zhang et al., 2004; McGraw
54 and Zhang, 2008).

55 The role of organic species in assisting aerosol nucleation and growth has been
56 demonstrated by both experimental and theoretical studies (Zhang et al., 2009; Zhao et al., 2009;
57 Wang et al., 2010; Xu et al., 2010b; Xu et al., 2012; Elm et al., 2014; Weber et al., 2014; Xu et
58 al., 2014; Zhu et al., 2014; Tröstl et al., 2016). However, the interactions between organic acids
59 and the other nucleation precursors are still elusive, due to the large variability in the
60 physicochemical nature of organic acids, e.g., the wide range of volatility and functionality
61 (Zhang et al., 2012; Riccobono et al., 2014). In addition, most of the previous theoretical studies
62 focus on the enhancement effects of organic acids on the SA-H_2O binary nucleation or the role of
63 organic acids in clustering basic species such as ammonia or amines with hydration (Zhao et al.,
64 2009; Xu et al., 2010; Xu et al. 2013; Elm et al., 2014; Weber et al., 2014; Zhu et al., 2014).
65 Several recent studies have been conducted on the underlying mechanisms of organic acids in
66 large pre-nucleation clusters (e.g. ammonia/amine-containing ternary nucleation) (Xu et al., 2010;
67 Xu et al., 2012; Elm et al., 2016a; Zhang et al., 2017), but most of these studies treated the
68 clusters without the consideration of hydration. Because of the ubiquitous presence of water (W)
69 in the atmosphere and its much higher abundance than other nucleation precursors, the hydration
70 effect on aerosol nucleation is significant (Loukonen et al., 2010; Xu and Zhang, 2013; Henschel
71 et al., 2014; Zhu et al., 2014; Henschel et al., 2016).

72 Atmospheric measurements have shown that the presence of dicarboxylic acids,
73 including succinic acid (SUA), is prevalent in ambient particles (Kawamura and Kaplan, 1987;
74 Decesari et al., 2000; Legrand et al., 2005; Hsieh et al. 2007; Blower et al., 2013). The effect of
75 dicarboxylic acids on aerosol nucleation involving SA or base molecules has been recognized in

theoretical studies. Xu and Zhang (2012) showed that dicarboxylic acids promote aerosol nucleation with other nucleating precursors in two directions via hydrogen bonding to the two carboxylic groups on dicarboxylic acids, which is distinct from monocarboxylic acids. Elm et al. (2014) indicated that clustering of a single pinic acid with SA molecules leads to closed structures because of no available sites for additional hydrogen bonding. In addition, Elm et al. (2017) suggested that more than two carboxylic acid groups are required for a given organic oxidation product to efficiently stabilize sulfuric-acid contained clusters. The interaction between SUA and dimethylamine (DMA) is strengthened by hydration via forming aminium carboxylate ion pairs (Xu and Zhang, 2013), while hydration of oxalic acid-AM cluster is unfavorable under atmospheric conditions (Weber et al., 2014). Clearly, the interactions of dicarboxylic acids with other nucleation precursors depend on the type of dicarboxylic acids and the number of the molecules involved in clustering. Presently, theoretical studies on the effect of dicarboxylic acids on nucleation from multi-component systems are lacking (Xu et al., 2010; Xu and Zhang, 2013). In particular, the role of organic acids as well as their participation in stabilizing larger pre-nucleation clusters of the SA-ammonia/amine systems needs to be evaluated with the presence of hydration in order to better understand NPF.

In this study, we performed theoretical calculations to evaluate the effect of SUA on hydrated SA•base clusters. Two base species, ammonia and dimethylamine (DMA), were considered. The Basin Paving Monte Carlo (BPMC) method was employed to sample stable cluster conformers, and quantum calculations were performed to predict the thermochemical properties of the multi-component clusters. Geometric and Topological analyses were carried out to investigate the structures and binding between SUA and SA•base clusters in the presence of

hydration. The implications of the interaction of SUA with hydrated SA-base clusters for atmospheric NPF are discussed.

2. COMPUTATIONAL METHODS

The methodology of the BPMC conformational sampling combined with quantum calculations using density functional theory (DFT) was employed to assess the role of SUA in clustering of SA with base compounds in the presence of water (Xu and Zhang, 2013). Briefly, the local energy minima in BPMC simulations was searched by using Amber11 package, and the Basin Hopping Monte Carlo (BHMC) approach was employed to increase the Monte Carlo transition probability, which allows the clustering system to escape from the traps of local energy minimum. We employed the Generalized Amber Force Field (GAFF) for AM, DMA and SUA following Wang et al. (2004; 2006). The force field parameters from Loukonen et al. (2010) were adapted for SUA and bisulfate ion. Hydration of the clustering system was evaluated by employing the TIP3P model. The geometric optimization and frequency calculations of the BPMC sampled cluster complexes were further performed at PW91PW91 level of theory with the basis set 6-311++G(2d, 2p) using Gaussian 09 software package (Frisch et al., 2009). Thermodynamic quantities, such as the electronic energy (ΔE with ZPE), enthalpy (ΔH), and Gibbs free energies (ΔG), were obtained on the basis of unscaled density functional frequencies at temperature of 298.15 K and pressure of 1 atm. Several basic cluster systems were also examined at the M06-2X/6-311++G(3df,3pd) level of theory, which has been suggested to be more reliable in predicting binary/ternary cluster formation (Elm and Mikkelsen, 2012; Leverentz et al., 2013; Zhang et al., 2017). Comparisons of the free energies with the two different DFT levels of theories between this study and previous available theoretical and experimental studies are presented in Table 1. The energies derived at the PW91PW91/6-

311++G(2d, 2p) are consistent with those of the M06-2X/6-311++G(3df,3pd) method, and the differences between our calculations and previous studies are within 1.6 kcal mol^{-1}. The thermochemical quantities calculated at the PW91PW91/6-311++G(2d, 2p) level of theory for the most stable cluster configurations are summarized in Table 2.

Topological analysis on the SA•base clusters with hydration and SUA was performed by employing the Multifunctional Wavefunction Analyzer (Multiwfn) 3.3.8 program (Lu and Chen, 2012). The topological characteristics at the bond critical points (BCPs) were calculated for electron density (ρ), Laplacian of electron density (Δρ), and potential energy density (*V*). Since the electron density is highly correlated to bonding strength (Lane et al., 2013), the potential energy density is an indicator of hydrogen bond energies (Espinosa et al., 1998). The occurrence of proton transfer in the clusters was determined using the localized orbital locator (LOL). A high LOL value denotes greatly localized electrons and indicates the existence of a covalent bond (Lu et al., 2012). The covalent bond is characterized by a negative Δρ, while a positive Δρ is associated with a hydrogen bond. In addition, a newly formed covalent bond via proton transfer was quantitatively examined in terms of the bond strength using the Laplacian bond order (LBO) as an indicator (Lu et al., 2013). Both LOL and LBO were calculated with Multiwfn 3.3.8 program (Lu et al., 2012).

The extent, to which clusters are hydrated (or the hydrophilicity of the clusters), is affected by humidity conditions in the atmosphere (Loukonenet al., 2010; Henschel et al., 2014; Henschel et al., 2016). To examine the influence of SUA on cluster hydration under different humidity conditions, the relative hydrate distributions over the number of water molecules contained in clusters were calculated at different relative humidity (RH) levels. The distribution was calculated according to Henschel et al. (2014), in which the Gibbs free energies of hydration

obtained from DFT calculations are converted to equilibrium constants for the formation of the respective hydrate by

$$K = e^{\frac{-\Delta G^0}{RT}} \quad (1)$$

and the relative hydrate population x_n of the hydrate containing n water molecules is determined by

$$x_n = \left(\frac{p(\mathrm{H_2O})}{p^0}\right)^n x_0 e^{\frac{-\Delta G_n}{RT}} \quad (2)$$

where $p(\mathrm{H_2O})$ is the water partial pressure, p^0 is the pressure of water at 1 atm, x_0 is the population of the dry cluster for $\sum_0^6 x_n = 1$, T is the standard temperature (298.15 K), and R is the molar gas constant. $p(\mathrm{H_2O})$ is related to RH through

$$p(\mathrm{H_2O}) = p(\mathrm{H_2O})_{eq} \times RH \quad (3)$$

where $p(\mathrm{H_2O})_{eq}$ is the water saturation vapor pressure, which is a function of the temperature (Wexler, 1976). Note that only the Gibbs free energy for the lowest energy structure for each hydration was considered and the Boltzmann averaging effect over configurations on comparable clusters was negligible for the free energies of hydration (Erupe et al., 2011; Xu and Zhang, 2013; Tsona et al., 2015).

To assess the importance of uptake of SUA on the SA•base clusters under atmospheric conditions, the ratio in the concentrations SA•X•SUA to $(SA)_2$•X (X denotes either AM or DMA) is estimated under equilibrium conditions,

$$\mathrm{SA \cdot X + SUA = SA \cdot X \cdot SUA} \quad (4)$$

$$\mathrm{SA \cdot X + SA = (SA)_2 \cdot X} \quad (5)$$

and the equilibrium constants K_1 and K_2 for reactions (4) and (5) are expressed as

$$K_1 = \frac{[\mathrm{SA \cdot X \cdot SUA}]}{[\mathrm{SA \cdot X}][\mathrm{SUA}]} = e^{\frac{-\Delta G_1}{RT}} \quad (6)$$

$$K_2 = \frac{[(\mathrm{SA})_2 \cdot \mathrm{X}]}{[\mathrm{SA} \cdot \mathrm{X}][\mathrm{SA}]} = e^{\frac{-\Delta G_2}{RT}} \quad (7)$$

The ratio between SA•X•SUA and $(SA)_2$•X concentrations is derived by dividing K_1 and K_2,

$$\frac{[SA \cdot X \cdot SUA]}{[(SA)_2 \cdot X]} = \frac{[SUA]}{[SA]} e^{\frac{-\Delta(\Delta G)}{RT}} \quad (8)$$

where $\Delta(\Delta G)$ is the difference in the Gibbs free energies between reactions (4) and (5) at 298 K. As listed in Table 3, the concentrations of sulfuric acid, ammonia, and dimethylamine in the atmosphere are typically in the range of $10^5 \sim 10^7$, $10^9 \sim 10^{11}$, $10^7 \sim 10^9$ molecules cm^{-3} (Zhang et al., 2012), and the SUA concentration is in the range of $10^8 \sim 10^9$ molecules cm^{-3} (Ho et al., 2007), resulting a SUA/SA ratio from 10 to 10^4. In addition, the concentration for the cluster $(SA)_m$•$(AM)_n$•$(DMA)_l$•$(SUA)_k$, [cluster], is estimated from the atmospheric concentrations of the various precursors,

$$[cluster] = [SA]^m \times [AM]^n \times [DMA]^l \times [SUA]^k \times e^{\left(\frac{-\Delta G}{RT}\right)} \quad (9)$$

where ΔG corresponds to the Gibbs free energy change for the reaction, mSA + nAM + lDMA + kSUA→ $(SA)_m$•$(AM)_n$•$(DMA)_l$•$(SUA)_k$.

3. RESULTS AND DISCUSSION

3.1 STRUCTURES AND TOPOLOGY

The most stable structures (in terms of ΔG at T = 298.15K and p = 1 atm) of the hydrated SA•base clusters are shown in Figures 1-3. Addition of SUA to hydrated SA•base clusters alters the hydrogen-bonding and rearranges the cluster structure, affecting the free energy and stability for the cluster formation.[15] Proton transfer occurs with SUA addition to SA•base, leading to a conversion from the hydrogen bond to covalent bond within the cluster. Proton transfer is absent in the SA•AM cluster (Figure 1a), consistent with the previous studies (Kurtén et al., 2006; Loukonen et al., 2010; Henschel et al., 2014), while the occurrence of proton transfer with SUA

addition (Figure 1b) is confirmed by the relocation of the LOL high value (Figure 4a). For the SA•AM cluster, a large value of LOL is adjacent to the SA molecule, indicating that electrons attained to the hydrogen atom (H1) on the S-O-H group are localized on the SA molecule side. In contrast, a large LOL region is located near the nitrogen atom (N1) on the AM molecule with the addition of SUA, suggesting that electrons are greatly localized on the AM side. Proton transfer converts the N1-H1 hydrogen bonding to a covalent bond, leading to the formation of ammonium bisulfate with a value of 0.464 for LBO. The formation of the covalent bond is also confirmed by the negative sign of $\nabla\rho$ at BCP of N1-H1 bond (Table S1). The electron density (potential energy density) at BCP of the N1-H1 bond exhibits a significant increase (decrease), from 0.091 (-0.087) a.u. in the SA•AM cluster to 0.271 (-0.424) a.u. in the SA•AM•SUA cluster. The structures of SA•AM and SA•DMA hydrates with up to five water molecules in our calculations are consistent with those of Henschel et al. (2014). The interactions between SA and AM/DMA in the presence of hydration were previously studied (DePalma et al., 2012; Yu et al., 2012; Qiu et al., 2013; Xu and Zhang, 2013; Tsona et al., 2015), showing strong hydrogen bonding among SA, base compound, and water molecules. Another study on glycolic acid found that addition of one glycolic acid molecule to the SA•AM cluster does not result in proton transfer, unless a second glycolic acid molecule is added (Zhang et al., 2017). Clearly, SUA is more efficient than glycolic acid to stabilize the SA•AM clusters.

In contrast to the SA•AM cluster, proton transfer occurs for the SA•DMA cluster without water or SUA (Figures 2 and 4b), because of stronger basicity of DMA than AM (Anderson et al., 2008). Similarly, proton transfer occurs for the SA•AM•DMA cluster, leading to the formation of the aminium bisulfate (HSO_4^-) ion pair. Addition of SUA to SA•DMA•AM•$(W)_n$ results in

additional proton transfer between the bisulfate ion and AM, leading to the formation of sulfate ions (SO_4^{2-}) (Figures 3 and 4c).

The dependence of the number of proton transfers on hydration is summarized in Table 4. For comparison, the results of hydration of SA clusters by Xu and Zhang (2013), who employed a similar method for the structure sampling and quantum calculations, are also included in this table. Both hydration and addition of SUA promote proton transfer in the SA•base clusters. Previous studies identified facile proton transfer by hydration (Ding et al., 2003; Al Natsheh et al., 2004; Loukonen et al., 2010; Xu and Zhang, 2013), and the dependence of proton transfer on the hydration level was also indicated by Tsona et al. (2015). For the SA cluster, Xu and Zhang (2013) found that proton transfer in the hydrated SA clusters only occurs with more than two water molecules. In our study, proton transfer due to hydration occurs in the monohydrate of SA•AM. A second proton transfer also occurs due to hydration, for example, when SA•AM•DMA•$(W)_5$ clusters are hydrated with one more water molecule (Figures 1a and 3a). The formation of the covalent bond in the monohydrate of SA•AM and the sixth hydrate of SA•AM•DMA is confirmed by the LOL relocation (Figure S1). Loukonen et al. (2010) also found that proton transfer occurs in SA•AM for the hydrated cluster with two water molecules. Our results show that neither water molecules nor SUA induce the second proton transfer in SA•DMA clusters. In contrast, Loukonon et al. (2010) showed that the second proton transfer occurs when the SA•DMA cluster is hydrated with five water molecules. The difference in proton transfer with hydration between this study and Loukonen et al. is attributable to the different sampling methodology used to obtain the most stable conformers of the clusters. Note that the findings of Loukonen et al. are also in contrast to those by Henschel et al. (2014).

Table 5 summarizes the available LBO values for the covalent bonds in the SA•base clusters with hydration. The dependence of LBO on the hydration level varies with the clusters. For SA•AM without SUA, additional water molecules result in higher LBO of N1-H1 bonds, while for SA•DMA LBO of the N2-H2 bond generally increases at all hydration levels except for the dihydrate. With addition of SUA to SA•AM and SA•DMA, the LBO values of the pre-existing covalent bonds of SUA-contained clusters are higher than those of the clusters without SUA at all hydration levels except for the sixth hydration. This indicates that, although addition of SUA to the two hydrated clusters does not result in additional proton transfer, the presence of SUA enhances the covalent bonds at the hydration levels of 0 to 5. The electron and the potential energy densities at BCPs of the N-H bonds are somewhat higher and lower, respectively, in the SUA-containing clusters than in those without SUA for most hydration cases (Tables S2 and S3).

Addition of SUA to SA•base results in cleavage of the hydrogen bond between the base and SA molecules (Figures 1b, 2b and 3b). Note that the carbon chain of SUA tends to bend accordingly as the hydration degree increases, because the carboxylic groups at the two ends of the carbon chain are involved in hydrogen bonding. As expected, the number of hydrogen bonds by AM in SA•AM•SUA clusters increases with the hydration degree, which is always equal or larger than that of the corresponding clusters without SUA and is closely related to the free energy changes of SUA addition to SA•AM clusters (see detailed discussions below on the energetics). For the DMA-containing clusters, the nitrogen atom is saturated by two hydrogen bonds, and the presence of the two free methyl groups likely corresponds to another factor affecting the stability (Ortega et al., 2012). The complexity of the cluster structures is partially ascribed by intramolecular hydrogen bonding associated with SUA, as illustrated by SA•AM•SUA•W, SA•DMA•SUA•W, or SA•AM•DMA•SUA•$(W)_5$ (Figures 1b, 2b and 3b).

3.2 ENERGETICS

The stepwise hydration free energies for the clusters, along with the number of water molecules in the clusters, are presented in Figure 5a and Table 2. For SA•AM and SA•DMA with up to five water molecules, the free energies are in agreement with those by Henschel et al. (2014) using the RICC2/aug-cc-pV(T+d)Z level for sulfur and the RICC2/aug-cc-pVTZ level for all other atoms, but differ from those by Loukonen et al. (2010) at the RI-MP2/aug-cc-pV(T+d)Z level of theory. Note that the structures of the hydrates in this study and Henschel et al. are different from those of Loukonen et al. (2010), explaining the differences in the energies among the various studies.

Figure 5a shows that the stepwise hydration energies are negative at most hydration degrees, suggesting that hydration is thermodynamically favorable. Without SUA, the fifth hydration of SA•AM and SA•DMA•AM and the sixth hydration of SA•DMA exhibit positive or nearly zero one step hydration free energies. These endergonic steps are ascribed because of the saturation by water molecules of the SA•base clusters (Henschel et al., 2013). For SUA-containing clusters, the addition of one more water molecule increases the free energy, resulting in a larger positive hydration energy. For example, the one step free energies are 2.99, 3.24 and 1.32 kcal mol^{-1} for the fifth hydration for SA•AM•SUA, the fourth hydration for SA•DMA•SUA, the third hydration of SA•DMA•AM•SUA, respectively. The large increases in free energies for SA•AM•SUA and SA•DMA•SUA are explained by structural rearrangement. The positive one-step hydration energy for the third hydration of SA•DMA•AM•SUA is likely because of the formation of the stable dihydrate.

The relative changes in the free energy due to addition of SUA to the SA•base clusters are depicted along with hydration degree (Figure 5b). For all hydration levels except the fourth

one, the free energy changes for the SA•DMA cluster by SUA addition are more negative than that for the SA•AM cluster, suggesting that the addition of SUA to SA•DMA is more favorable than that to SA•AM. The largest change in the free energy (-7.15 kcal mol^{-1}) between SA•AM•SUA and SA•AM occurs at the fourth hydration step, which is attributable to the structure change due to SUA addition, i.e., an additional hydrogen bond formed on AM in the fourth hydrate of SA•AM•SUA. However, such a hydrogen bond is absent in the SA•AM cluster until the fifth hydration (Figure 1). The largest negative free energy change (-9.86 kcal mol^{-1}) in SA•DMA corresponds to the unhydrated form. The strong hydrogen bonds between DMA and the two acids formed in the unhydrated SA•DMA•SUA cluster undergo cleavage due to water uptake, leading to a smaller free energy difference between the SA•DMA•SUA and SA•DMA clusters with hydration. In addition, stabilization by hydration for the SA•base clusters is weakened by addition of SUA, particularly for the SA•DMA and SA•DMA•AM clusters, with much smaller hydration energies for SA•DMA•SUA and SA•DMA•AM•SUA than the corresponding clusters without SUA (Fig. 5a). It is evident that the Gibbs free energy changes of SUA addition to the multi-component clusters are relevant to the hydration degree and the base types.

The role of SUA in the subsequent growth of the SA•base clusters was examined by comparing the differences in free energies for adding SA to SA•DMA and SA•DMA•SUA. Computations were also performed for the unhydrated $(SA)_2$•DMA, $(SA)_3$•DMA and $(SA)_2$•DMA•SUA clusters (Table 6). The optimized clusters containing more than one SA molecules are depicted in Figure 6. The free energies of SA addition to SA•DMA and $(SA)_2$•DMA are -10.5 and -6.1 kcal mol^{-1}, respectively. The free energy for adding SA to SA•DMA•SUA is -5.14 kcal mol^{-1}, higher than that of SA addition to SA•DMA. With hydration

301 (i.e., $(SA)_2$•DMA•SUA•(W)x), the free energies for adding SA to SA•DMA•SUA•(W)x clusters
302 are all negative (Table 2).

303 **3.3 HYDRATION PROFILES**

304 The equilibrium hydrate distributions were calculated for the SA•base clusters with and
305 without the presence of SUA. Figure 7 displays the relative hydrate distributions under three
306 typical atmospheric RH values, i.e., 20%, 50% and 80%. The SA•base cluster shows an
307 increasing hydration with increasing RH, although the different clusters exhibit distinct
308 characteristics in the hydrate distribution.

309 Our results for the SA•AM hydrate distribution are consistent with the previous studies
310 (Loukonen et al., 2010; Henschel et al., 2014), showing that the hydrate distribution of SA•AM
311 is sensitive to RH (Figure 7a). The completely dry SA•AM cluster dominates the hydrate
312 distribution under low RH (<40%), while the trihydrate is most prevalent as RH exceeds 40%
313 because of higher stability of the trihydrate than the monohydrate and dihydrate. Since the
314 change in the free energies is almost identical for addition of 1 or 2 water molecules, the
315 SA•DMA clusters of the unhydrated form, monohydrate, and dihydrate are evenly distributed
316 (Figure 7b) and account for 85% of the total population at all RH levels. The peak of the hydrate
317 distribution for SA•DMA shows a continuous shift from the unhydrated cluster to dihydrate with
318 increasing RH. The SA•DMA•AM cluster tends to be dehydrated, as reflected by the fact that the
319 relative population of dry SA•DMA•AM clusters exceeds 50% even under highly humid
320 conditions (Figure 7c). Hence, addition of DMA or AM considerably lowers the hydrophilicity
321 of SA•AM or SA•DMA. The dehydration trend of the SA•DMA•AM cluster in our work is
322 consistent with the previous investigations,[31] in which the base-containing clusters with SA were
323 found to be less hydrophilic than the SA clusters.

Addition of SUA alters the hydrate distribution of the SA•base clusters. For example, the hydrate distribution is broader for SA•AM•SUA than for SA•AM (Figure 7a,d), with a considerably high population of the fourth hydrate for SA•AM•SUA at high RH to promote hydration. The broader hydrate distribution is consistent with the more negative hydration energy at the fourth hydration step for SA•AM•SUA for SA•AM. However, the peaks of the distribution exhibit a similar pattern with varying RH for SA•AM and SA•AM•SUA, i.e., with unhydrated and trihydrate clusters as the most populated forms. The hydrate distributions for SA•DMA•SUA and SA•DMA exhibit distinct characteristics. In the presence of SUA, over 80% of the clusters exist in a dry state independent on RH (Figure 7e), indicating that hydration of SA•DMA•SUA is less favorable than that of SA•DMA. The hydrate distribution peak for SA•DMA•SUA at the unhydrated cluster is consistent with that addition of SUA greatly reduces the free energy of the dry clusters and the changes in hydration free energy are relatively small at all hydration levels. The SA•DMA•AM•SUA clusters are likely dehydrated or hydrated with two water molecules dependent on RH (Figure 7f), as the distribution peak shifts between the unhydrated (RH < 70%) and the dihydrate (RH >70%) clusters and does not exhibit a peak on monohydrate at any RH level. Clearly, hydration is more favorable for SA•DMA•AM•SUA than for SA•DMA•AM.

The hydration profiles are shown in Figure 8 as functions of RH for the clusters with SA•base. The maximal numbers of water molecules for SA•AM, SA•DMA, and SA•DMA•AM are 2.7, 1.7, and 0.9, respectively, as RH approaches 100%. The calculated degrees of hydration for SA•AM and SA•DMA are slightly higher by this study than those by Henschel et al. (2014) Addition of SUA considerably enhances the hydrophilicity of SA•AM and SA•DMA•AM, leading to high degrees of hydration for SUA-containing clusters. In contrast, the number of

water molecules bound to SA•DMA is greatly reduced with SUA addition, since the most populated cluster of SA•DMA•SUA is unhydrated for different RH (Figure 7e).

3.4 ATMOSPHERIC IMPLICATIONS

The cluster growth can be represented by a reversible, stepwise kinetic process in a single or multi-component system (Zhang et al., 2012),

$$...C_{i-1} \underset{k_i^-}{\overset{+A_{i-1},k_{i-1}^+}{\rightleftarrows}} C_i \underset{k_{i+1}^-}{\overset{+A_i,k_i^+}{\rightleftarrows}} C_{i+1}... \quad (10)$$

where $A_{i\text{-}1}$ denotes a monomer species to be added to the cluster $C_{i\text{-}1}$ at the $(i-1)^{th}$ step and k_i^- and k_i^+ represent the association and decomposition rate constants of the cluster, respectively. Hence, whether cluster C_i grows or decomposes is dependent on the competition between the forward and backward reactions for C_i, which are dependent on the rate constant k_i^+ and monomer concentration $[A_i]$ and k_i^- (i.e., the thermal stability of C_i, respectively. The time-dependent concentration of cluster C_i is derived according to (Zhang et al., 2012),

$$\frac{d[C_i]}{dt} = k_{i-1}^+[C_{i-1}][A_{i-1}] - k_i^-[C_i] - k_i^+[C_i][A_i] + k_{i+1}^-[C_{i+1}] \quad (11)$$

Note that the eq. 9 is the steady-state expression of eq.11 summed over all reaction steps.

Addition of SUA to SA or SA•base is thermodynamically favorable (Figure 5b), as reflected by large negative free energies. The estimated cluster concentrations using eq. 9 and the atmospherically relevant concentrations of the precursor species are 10^{-3} ~10^2 cm^{-3} for SA•DMA•SUA and 10^0 ~10^3 cm^{-3} for SA•SUA (Table 6), suggesting that SUA likely contributes to the further growth of the SA and SA•base clusters. Furthermore, the dipole moments of SA•DMA•SUA and SA•AM•SUA are 7.5 and 8.8 Debye, respectively (Table 6), which are the largest among those of the trimers. The calculated ratios of [SA•X•SUA]/[$(SA)_2$•X] (X denotes AM, DMA, water molecule, or none) under atmospherically relevant concentrations are

368 presented in Table 7. The estimated ratio of [SA•DMA•SUA] to [$(SA)_2$•DMA] is in the range
369 from 3:1 to 3000:1 under atmospherically relevant concentrations for the precursor species, i.e.,
370 [SUA]/[SA] in the range from 10:1 to 10^4:1, indicating that SA•DMA•SUA is prevalent in the
371 atmosphere. The ratios of [SA•SUA]/[$(SA)_2$] and [SA•W•SUA]/[$(SA)_2$•W] are both higher than
372 10^3:1, indicating that the SUA-containing clusters are prevalent for both unhydrated and
373 hydrated SA clusters with one water molecule. While sulfuric acid dimer is believed to be an
374 important precursor for NPF (Zhang et al., 2012), our study shows that SUA, which is one of
375 most abundant dicarboxylic acids in atmosphere, competes with the formation and further
376 growth of sulfuric acid dimer because of the strong interaction of SUA with SA to form the
377 unhydrated or hydrated clusters. The effect of SUA on the formation and further growth of
378 sulfuric acid dimer is more pronounced than that by ketodiperoxy acid (Elm et al., 2016b). Fig.
379 9 depicts the relative stability of cluster formation from the interaction among SUA, SA, base,
380 and W molecules, showing SA•DMA as the most stable dimer and $(SA)_2$•DMA as most stable
381 trimer, following by SA•DMA•SUA.

382 It should be pointed out that steady-state equilibrium for pre-nucleation clusters is rarely
383 established under atmospheric conditions for each intermediate step (i.e., eq. 11) and the overall
384 cluster growth (i.e., eq. 9), because of continuous forward reactions by adding monomers to form
385 larger clusters during NPF. Whether a cluster grows to form a nanoparticle is dependent on the
386 competition between the forward reaction by adding a monomer and the backward reaction by
387 losing a monomer (evaporation) at each intermediate step. For example, at step *i* the cluster
388 grows (or evaporates) when the term of k_i^+ x $[A_i]$ is larger (smaller) than that of k_i^- (eq. 11).
389 While the evaporation rate relies on the thermodynamic stability of the cluster, the forward rate
390 constant is kinetically controlled, dependent on the interaction (i.e., the natural charges and

dipole moments) and kinetical energies between the colliding cluster and monomer (Zhang et al., 2012). For neutral clusters, electrostatically-induced dipole-dipole interaction plays a key role in facilitating the forward reaction rate. The presence of organic acids typically increases the dipole moment of clusters (Zhao et al., 2009). Furthermore, in addition to SUA, there are many other organic acids present under ambient conditions. In particular, organic acids with multi-functionality, i.e., more carboxylic acid groups and the presence of hydroxyl groups, likely contribute more importantly to aerosol nucleation.

4. CONCLUSIONS

We have investigated the molecular interactions between SUA and SA•base clusters in the presence of hydration, including AM and DMA. SUA addition promotes proton transfer in the SA•base clusters, which is confirmed by formation of new covalent bonds and relocation of the high LOL value from the SA side to the AM side and a shift from positive to negative for the Laplacian of electron density. The presence of SUA in SA•AM and SA•DMA clusters generally strengthens the existing covalent bonds in SA•base•SUA•$(W)_n$ clusters at the various hydration levels, since the LBO values of the covalent bonds in SUA-containing clusters are higher than those in the clusters without SUA. The hydrate distribution is broader for SA•AM•SUA than for SA•AM. Also, the peak in the distribution of SA•DMA•AM•SUA hydrates occurs at the two-water molecule level under high RH, but the peak in the distribution for SA•DMA•AM corresponds to the unhydrated cluster. The peak hydrate distribution shifts toward a larger number of water molecules in SUA-containing clusters than in clusters without SUA, suggesting that the addition of SUA enhances the hydrophilicity of SA•AM and SA•DMA•AM. However, the presence of SUA causes dehydration to the SA•DMA clusters, since the most prevalent cluster for SA•DMA•SUA is in a dry state. At equilibrium and atmospherically typical

414 abundances of SUA and SA, SUA•SA•base (AM or DMA) is the most dominant form among the
415 three-molecule clusters, indicating that SUA competes with SA for the growth of the SA•base
416 dimers.

417 Various organic acids are produced from atmospheric oxidation of volatile organic
418 compounds from biogenic (i.e., pinenes) and anthropogenic sources (i.e., aromatics). Our results
419 indicate that the multi-component molecular interaction involving organic acids, sulfuric acid,
420 and base species promotes NPF in the atmosphere, particularly under polluted environments
421 because of elevated concentrations of these species. The role of different organic acids with
422 distinct functionality in NPF needs to be further assessed. In particular, future studies are
423 necessary to evaluate both the kinetics and thermodynamics of the interactions of organic acids
424 with SA and base species, i.e., the forward and reverse rates as well as the potential energy
425 surfaces for cluster formation, in order to develop physically-based parameterizations of NPF in
426 atmospheric models.

427 **SUPPLEMENTARY MATERIAL**

428 Supplementary material contains additional relief maps for the sulfuric acid-base clusters
429 and lists of topological properties for the most stable conformers of each cluster categories.

430 **ACKNOWLEDGMENTS**

431 This work was supported by National Natural Science Foundation of China (41675122,
432 41425015, U1401245, and 41373102), Science and Technology Program of Guangzhou City
433 (201707010188), Team Project from the Natural Science Foundation of Guangdong Province,
434 China (S2012030006604), Special Program for Applied Research on Super Computation of the
435 NSFC-Guangdong Joint Fund (the second phase), National Super-computing Centre in
436 Guangzhou (NSCC-GZ), and Robert A. Welch Foundation (A-1417). The research was partially

conducted with the advanced computing resources provided by Texas A&M High Performance Research Computing. The authors acknowledged the Laboratory for Molecular Simulations at Texas A&M University.

References

Andreae, M. O., Rosenfeld, D., Artaxo, P., Costa, A. A., Frank, G. P., Longo, K. M., and Silva-Dias, M. A. F.: Smoking rain clouds over the Amazon, Science, 303, 1337–1342, 2004.

Anderson, K. E., Siepmann, J. I., McMurry, P. H., and VandeVondele, J.: Importance of the Number of Acid Molecules and the Strength of the Base for Double-Ion Formation in (H2SO4)m•Base•(H2O)6 Clusters, J. Am. Chem. Soc., 130, 14144–14147, https://doi.org/10.1021/ja8019774, 2008.

Al Natsheh, A., Nadykto, A. B., Mikkelsen, K. V., Yu, F., and Ruuskanen, J.: Sulfuric acid and sulfuric acid hydrates in the gas phase: A DFT investigation, J. Phys. Chem. A, 108, 8914–8929, https://doi.org/10.1021/jp048858o, 2004.

Bianchi, F., Tröstl, J., Junninen, H., Frege, C., Henne, S., Hoyle, C. R., Molteni, U., Herrmann, E., Adamov, A., Bukowiecki, N., Chen, X., Duplissy, J., Gysel, M., Hutterli, M., Kangasluoma, J., Kontkanen, J., Kürten, A., Manninen, H. E., Münch, S., Peräkylä, O., Petäjä, T., Rondo, L., Williamson, C., Weingartner, E., Curtius, J., Worsnop, D. R., Kulmala, M., Dommen, J., and Baltensperger, U.: New particle formation in the free troposphere: A question of chemistry and timing, Science, 352, 1109–1112, https://doi.org/10.1126/science.aad5456, 2016.

Blower, P. G., Ota, S. T., Valley, N. A., Wood, S. R., and Richmond, G. L.: Sink or Surf: Atmospheric Implications for Succinic Acid at Aqueous Surfaces, J. Phys. Chem. 117, 7887–7903, https://doi.org/10.1021/jp405067y, 2013.

Cai, R., and Jiang, J.: A new balance formula to estimate new particle formation rate: reevaluating the effect of coagulation scavenging, Atmos. Chem. Phys., 17, 12659-12675, https://doi.org/10.5194/acp-17-12659-2017, 2017.

464 Decesari, S., Facchini, M. C., Fuzzi, S., and Tagliavini, E., Characterization of water-soluble
465 organic compounds in atmospheric aerosol: A new approach, J. Geophys. Res. Atmos., 105,
466 1481-1489, https://doi.org/10.1029/1999JD900950, 2000.
467 DePalma, J. W., Bzdek, B. R., Doren, D. J., and Johnston, M. V.: Structure and energetics of
468 nanometer size clusters of sulfuric acid with ammonia and dimethylamine, J. Phys. Chem. A
469 116, 1030–1040, https://doi.org/10.1021/jp210127w, 2012.
470 Ding, C.-G., Laasonen, K., and Laaksonen, A.: Two sulfuric acids in small water clusters, J.
471 Phys. Chem. 107, 8648–8658, https://doi.org/10.1021/jp022575j, 2003.
472 Elm, J., Bilde, M., and Mikkelsen, K. V.: Assessment of density functional theory in predicting
473 structures and free energies of reaction of atmospheric prenucleation clusters, J. Chem.
474 Theory and Comp., 8, 2071–2077, https://doi.org/10.1021/ct300192p, 2012.
475 Elm, J., Kurten, T., Bilde, M., and Mikkelsen, K. V.: Molecular interaction of pinic acid with
476 sulfuric acid: exploring the thermodynamic landscape of cluster growth, J. Phys. Chem. A,
477 118, 7892-7900, https://doi.org/10.1021/jp503736s (2014).
478 Elm, J., Jen, C. N., Kurtén, T., and Vehkamäki, H.: Strong hydrogen bonded molecular
479 interactions between atmospheric diamines and sulfuric acid, J. Phys. Chem., 120, 3693–
480 3700, https://doi.org/10.1021/acs.jpca.6b03192, 2016a.
481 Elm, J., Myllys, N., Luy, J.-N., Kurtén, T., and Vehkamäki, H.: The Effect of Water and Bases
482 on the Clustering of a Cyclohexene Autoxidation Product C6H8O7 with Sulfuric Acid, J.
483 Phys. Chem., 120, 2240–2249, https://doi.org/10.1021/acs.jpca.6b00677, 2016b.
484 Elm, J., Myllys, N., and Kurtén, T.: What is required for highly oxidized molecules to form
485 clusters with sulfuric acid? J. Phys. Chem., 121 (23), 4578-4587, doi:
486 10.1021/acs.jpca.7b03759, 2017.

Erupe, M. E., Viggiano, A. A., and Lee, S.-H.: The effect of trimethylamine on atmospheric nucleation involving H2SO4, Atmos. Chem. Phys., 11, 4767-4775, https://doi.org/10.5194/acp-11-4767-2011, 2011.

Espinosa, E., Molins, E., and Lecomte, C.: Hydrogen bond strengths revealed by topological analyses of experimentally observed electron densities, Chem. Phys. Lett. 285, 170-173, https://doi.org/10.1016/S0009-2614(98)00036-0, 1998.

Fan, J., Zhang, R., Li, G., and Tao, W.-K.: Effects of aerosols and relative humidity on cumulus clouds, J. Geophys. Res., 112, D14204, https://doi.org/10.1029/2006JD008136, 2007.

Frisch, M. J., Trucks, G. W., Schlegel, H. B., Scuseria, G. E., Robb, M. A., Cheeseman, J. R., Scalmani, G., Barone, V., Petersson, G. A., Nakatsuji, H., Li, X., Caricato, M., Marenich, A., Bloino, J., and Janesko, R. G. B. G., Mennucci, B., Hratchian, H. P., Ortiz, J. V., Izmaylov, A. F., Sonnenberg, J. L., Williams-Young, D., Ding, F., Lipparini, F., Egidi, F., Goings, J., Peng, B., Petrone, A., Henderson, T., Ranasinghe, D., Zakrzewski, V. G., Gao, J., Rega, N., Zheng, G., Liang, W., Hada, M., Ehara, M., Toyota, K., Fukuda, R., Hasegawa, J., Ishida, M., Nakajima, T., Honda, Y., Kitao, O., Nakai, H., Vreven, T., Throssell, K., Montgomery Jr., J. A., Peralta, J. E., Ogliaro, F., Bearpark, M., Heyd, J. J., Brothers, E., Kudin, K. N., Staroverov, V. N., Keith, T., Kobayashi, R., Normand, J., Raghavachari, K., Rendell, A., Burant, J. C., Iyengar, S. S., Tomasi, J., Cossi, M., Millam, J. M., Klene, M., Adamo, C., Cammi, R., Ochterski, J. W., Martin, K. R. L., Morokuma, Farkas, O., Foresman, J. B., and Fox, D. J.: Gaussia, Gaussian 09, Revision A.02 (Gaussian, Inc., Wallingford CT, 2009).

Ge, X., Wexler, A. S., Clegg, S. L.: Atmospheric amines – Part I. A review, Atmos. Environ., 45, 524, http://doi.org/10.1016/j.atmosenv.2010.10.012, 2011.

509 Guo, S., Hu, M., Zamora, M. L., Peng, J., Shang, D., Zheng, J., Du, Z., Wu, Z., Shao, M., Zeng,
510 L., Molina, M.J., and Zhang, R.: Elucidating severe urban haze formation in China, Proc.
511 Natl. Acad. Sci. USA, 111, 17373–17378, https://doi.org/10.1016/10.1073/pnas.1419604111,
512 2014.
513 Hanson, D. R., and Eisele, F. L.: Acid–base chemical reaction model for nucleation rates in the
514 polluted atmospheric boundary layer, J. Geophys. Res. Atmos., 107, 18713-18718,
515 https://doi.org/10.1073/pnas.1210285109, 2002.
516 Henschel, H., Ortega, I. K., Kupiainen, O., Olenius, T., Kurtén, T., and Vehkamäki, H.:
517 Hydration of pure and base-Containing sulfuric acid clusters studied by computational
518 chemistry methods, AIP Conference Proceedings, 1527, 218-221,
519 https://doi.org/10.1063/1.4803243, 2013.
520 Henschel, H., T. Kurtén, and Vehkamäki, H.: Hydration of Atmospherically Relevant Molecular
521 Clusters: Computational Chemistry and Classical Thermodynamics, J. Phys. Chem., 120,
522 2599–2611, https://doi.org/10.1021/jp500712y, 2016.
523 Henschel, H., Navarro, J. C., Yli-Juuti, T., Kupiainen-Maatta, O., Olenius, T., Ortega, I. K.,
524 Clegg, S. L., Kurten, T., Riipinen, I., and Vehkamaki, H.: Hydration of atmospherically
525 relevant molecular clusters: Computational chemistry and classical thermodynamics, J. Phys.
526 Chem. A, 118, 2599-2611, https://doi.org/10.1021/jp500712y, 2014.
527 Ho, K. F., Cao, J. J., Lee, S. C., Kawamura, K., Zhang, R. J. , Chow, J. C., and Watson, J.
528 G.: Dicarboxylic acids, ketocarboxylic acids, and dicarbonyls in the urban atmosphere of
529 China, J. Geophys. Res., 112, D22S27, https://doi.org/10.1029/2006JD008011, 2007.
530 Hsieh, L.-Y., Kuo, S.-C., Chen, C.-L., and Tsai, Y. I.: Origin of Low-molecular-weight
531 Dicarboxylic Acids and their Concentration and Size Distribution Variation in Suburban

Aerosol, Atmos. Environ., 41, 6648–6661, https://doi.org/10.1016/j.atmosenv.2007.04.014 2007.

IPCC, Climate Change 2013: The Physical Science Basis. Contribution of Working Group I to the Fifth Assessment Report of the Intergovernmental Panel on Climate Change (Cambridge University Press, Cambridge, United Kingdom and New York, NY, USA: http://www.ipcc.ch/report/ar5/wg1/, 2013).

Kawamura, K., and Kaplan, I. R.: Motor exhaust emissions as a primary source for dicarboxylic acids in Los Angeles ambient air, Environ. Sci. Technol., 21, 105-110, 1987.Legrand, M., Preunkert, S., Galy-Lacaux, C., Liousse, C., and Wagenbach, D.: J. Geophys. Res.: Atmospheric year‐round records of dicarboxylic acids and sulfate at three French sites located between 630 and 4360 m elevation, Atmos. 110, https://doi.org/10.1029/2004JD005515, 2005.

Kuang, C., Riipinen, I., Sihto, S.-L., Kulmala, M., McCormick, A. V., and McMurry, P. H.: An improved criterion for new particle formation in diverse atmospheric environments, Atmos. Chem. Phys., 10, 8469–8480, doi:10.5194/acp-10-8469-2010, 2010.

Kulmala, M. and Kerminen, V. M.: On the formation and growth of atmospheric nanoparticles, Atmos. Res., 90, 132–150, https://doi.org/10.1016/j.atmosres.2008.01.005, 2008.

Kurtén, T., Sundberg, M. R., Vehkamäki, H., Noppel, M., Blomqvist, J., and Kulmala, M.: Ab initio and density functional theory reinvestigation of gas-phase sulfuric acid monohydrate and ammonium hydrogen sulfate, J. Phys. Chem. https://doi.org/110, 7178–7188, 10.1021/jp0613081, 2006.

553 Lane, J. R., Contreras-García, J., Piquemal, J.-P., Miller, B. J., and Kjaergaard, H. G.: Are bond
554 critical points really critical for hydrogen bonding? J. Chem. Theory and Comp. 9, 3263–
555 3266, https://doi.org/10.1021/ct400420r, 2013.
556 Lee, S. H., Reeves, J. M., Wilson, J. C., Hunton, D. E., Vig- giano, A. A., Miller, T. M.,
557 Ballenthin, J. O., and Lait, L. R.: Particle formation by ion nucleation in the upper tro-
558 posphere and lower stratosphere: Science, 301, 1886–1889,
559 https://doi.org/10.1126/science.1087236, 2003.
560 Leverentz, H. R., Siepmann, J. I., Truhlar, D. G., Loukonen, V., and Vehkamäki, H.: Energetics
561 of atmospherically implicated clusters made of sulfuric acid, ammonia, and dimethyl amine,
562 J. Phys. Chem. A, 117, 3819–3825, https://doi.org/10.1021/jp402346u, 2013.
563 Li, G., Wang, Y., and Zhang, R.: Implementation of a two-moment bulk microphysics scheme to
564 the WRF model to investigate aerosol-cloud interaction, J. Geophys. Res. 113, D15211,
565 https://doi.org/10.1029/2007JD009361, 2008.
566 Loukonen, V., Kurtén, T., Ortega, I. K., Vehkamäki, H., Pádua, A. A. H., Sellegri, K., Kulmala,
567 M.: Enhancing effect of dimethylamine in sulfuric acid nucleation in the presence of water –
568 a computational study, Atmos. Chem. Phys., 10, 4961-4974, https://doi.org/10.5194/acp-10-
569 4961-2010, 2010.
570 Lu, T., and Chen, F.: Multiwfn: A multifunctional wavefunction analyzer, J. Comput. Chem. 33,
571 580-592, https://doi.org/10.1002/jcc.22885, 2012.
572 Lu, T., and Chen, F.: Bond order analysis based on the Laplacian of electron density in fuzzy
573 overlap space, J. Phys. Chem. A, 117, 3100–3108, https://doi.org/10.1021/jp4010345, 2013.

McGraw, R., and Zhang, R.: Multivariate analysis of homogeneous nucleation rate measurements: I. Nucleation in the p-toluic acid/sulfuric acid/water system, J. Chem. Phys. 128, 064508, https://doi.org/10.1063/1.2830030, 2008.

Merikanto, J., Spracklen, D. V., Mann, G. W., Pickering, S. J., and Carslaw, K. S.: Impact of nucleation on global CCN, Atmos. Chem. Phys., 9, 8601-8616, https://doi.org/10.5194/acp-9-8601-2009, 2009.

Nadykto, A. B., and Yu, F.: Strong hydrogen bonding between atmospheric nucleation precursors and common organics, Chem. Phys. Lett., 435, 14-18, https://doi:.org/10.1016/j.cplett.2006.12.050, 2007.

Nadykto, A.B., Yu, F., Jakovleva, M.V., Herb, J., and Xu, Y.: Amines in the Earth's Atmosphere: A Density Functional Theory Study of the Thermochemistry of Pre-Nucleation Clusters, Entropy, 13, 554–569, https://doi.org/10.3390/e13020554, 2011.

Qiu, C., and Zhang, R.: Multiphase chemistry of atmospheric amines, Phys. Chem. Chem. Phys., 15, 5738-5752, https://doi.org/10.1039/C3CP43446J, 2013.

Ortega, I. K., Kupiainen, O., Kurtén, T., Olenius, T., Wilkman, O., McGrath, M. J., Loukonen, V., and Vehkamäki, H.: From quantum chemical formation free energies to evaporation rates, Atmos. Chem. Phys., 12, 225-235, https://doi.org/10.5194/acp-12-225-2012, 2012.

Riccobono, F., Schobesberger, S., Scott, C. E., Dommen, J., Ortega, I. K., Rondo, L., Almeida, J., Amorim, A., Bianchi, F., Breitenlechner, M., David, A., Downard, A., Dunne, E. M., Duplissy, J., Ehrhart, S., Flagan, R. C., Franchin, A., Hansel, A., Junni- nen, H., Kajos, M., Keskinen, H., Kupc, A., Kürten, A., Kvashin, A. N., Laaksonen, A., Lehtipalo, K., Makhmutov, V., Mathot, S., Nieminen, T., Onnela, A., Petäjä, T., Praplan, A. P., Santos, F. D., Schallhart, S., Seinfeld, J. H., Sipilä, M., Spracklen, D. V., Stozhkov, Y., Stratmann, F.,

Tomé, A., Tsagkogeorgas, G., Vaattovaara, P., Viisanen, Y., Vrtala, A., Wagner, P. E., Weingart- ner, E., Wex, H., Wimmer, D., Carslaw, K. S., Curtius, J., Donahue, N. M., Kirkby, J., Kulmala, M., Worsnop, D. R., and Baltensperger, U.: Oxidation products of biogenic emissions contribute to nucleation of atmospheric particles, Science 344, 717-721, https://doi.org/10.1126/science.1243527, 2014.

Rychlik, K., Secrest, J. R., Lauc, C., Pulczinski, J., Zamora, M. L., Leal, J., Langleya, R., Myatt, L., Raju, M., Chang, R. C.-A., Li, Y., Golding, M.C., Rodrigues-Hoffmann, A., Molina, M.J., Zhang, R. and Johnson, N.M.: In utero ultrafine particulate matter exposure causes offspring pulmonary immunosuppression, Proc. Natl. Acad. Sci. USA 116, 3443–3448, doi/10.1073/pnas.1816103116, 2019.

Tröstl, J., Chuang, W. K., Gordon, H., Heinritzi, M., Yan, C., Molteni, U., Ahlm, L., Frege, C., Bianchi, F., Wagner, R., Si- mon, M., Lehtipalo, K., Williamson, C., Craven, J. S., Du- plissy, J., Adamov, A., Almeida, J., Bernhammer, A.-K., Bre- itenlechner, M., Brilke, S., Dias, A., Ehrhart, S., Flagan, R. C., Franchin, A., Fuchs, C., Guida, R., Gysel, M., Hansel, A., Hoyle, C. R., Jokinen, T., Junninen, H., Kangasluoma, J., Kesk- inen, H., Kim, J., Krapf, M., Kürten, A., Laaksonen, A., Lawler, M., Leiminger, M., Mathot, S., Möhler, O., Nieminen, T., On- nela, A., Petäjä, T., Piel, F. M., Miettinen, P., Rissanen, M. P., Rondo, L., Sarnela, N., Schobesberger, S., Sengupta, K., Sip- ilä, M., Smith, J. N., Steiner, G., Tomè, A., Virtanen, A., Wag- ner, A. C., Weingartner, E., Wimmer, D., Winkler, P. M., Ye, P., Carslaw, K. S., Curtius, J., Dommen, J., Kirkby, J., Kulmala, M., Riipinen, I., Worsnop, D. R., Donahue, N. M., and Bal- tensperger, U.: The role of low-volatility organic compounds in initial particle growth in the atmosphere, Nature, 533, 527-531, https://doi.org/10.1038/nature18271, 2016.

620 Tsona, N. T., Henschel, H., Bork, N., Loukonen, V., and Vehkamäki, H.: Structures, Hydration,
621 and Electrical Mobilities of Bisulfate Ion–Sulfuric Acid–Ammonia/Dimethylamine Clusters:
622 A Computational Study, J. Phys. Chem. A, 119, 9670–9679,
623 https://doi.org/10.1021/acs.jpca.5b03030, 2015.
624 Wang, L., Khalizov, A.F., Zheng, J., Xu, W., Lal, V., Ma, Y., and Zhang, R.: Atmospheric
625 nanoparticles formed from heterogeneous reactions of organics, Nature Geosci., 3, 238-242,
626 https://doi.org/10.1038/ngeo778, 2010.
627 Wang, J., Krejci, R., Giangrande, S., Kuang, C., Barbosa, H. M. J., Brito, J., Carbone, S., Chi,
628 X., Comstock, J., Ditas, F., Lavric, J., Manninen, H. E., Mei, F., Moran-Zuloaga, D.,
629 Pöhlker, C., Pöh- lker, M. L., Saturno, J., Schmid, B., Souza, R. A. F., Springston, S. R.,
630 Tomlinson, J. M., Toto, T., Walter, D., Wimmer, D., Smith, J. N., Kulmala, M., Machado,
631 L. A. T., Artaxo, P., Andreae, M. O., Petäjä, T., and Martin, S. T.: Amazon boundary layer
632 aerosol concentration sustained by vertical transport during rainfall, Na- ture, 539, 416–419,
633 https://doi.org/10.1038/nature19819, 2016.
634 Wang, C.-Y., Jiang, S., Liu, Y.-R., Wen, H., Wang, Z.-Q., Han, Y.-J., Huang, T., Huang, W.:
635 Synergistic Effect of Ammonia and Methylamine on Nucleation in the Earth's Atmosphere.
636 A Theoretical Study, J. Phys. Chem. A, 122, 3470−3479, https://doi.org/
637 10.1021/acs.jpca.8b0068, 2018.
638 Wang, Z. B., Hu, M., Mogensen, D., Yue, D. L., Zheng, J., Zhang, R., Liu, Y., Yuan, B., Li, X.,
639 Shao, M., Zhou, L., Wu, Z. J., Wiedensohler, A. and Boy, M.: The simulations of sulfuric
640 acid concentration and new particle formation in an urban atmosphere in China, Atmos.
641 Chem. Phys. 13, 11157-11167, doi:10.5194/acp-13-11157-2013, 2013.

642 Weber, R. J., P. H. McMurry, R. L. Mauldin III, D. J. Tanner, F. L. Eisele, A. D. Clarke, and
643 Kapustin V. N.: New Particle Formation in the Remote Troposphere: A Comparison of
644 Observations at Various Sites, Geophys. Res. Lett., 26(3), 307-310,
645 doi:10.1029/1998GL900308, 1999.
646 Wexler, A.: Vapor pressure formulation for water in range 0 to 100 C. A revision, J. Res. Nat.
647 Bur. Stand. 80A, 775-785, 1976.
648 Xu, Y., Nadykto, A. B., Yu, F., Jiang, L., and Wang, W.: Formation and properties of hydrogen-
649 bonded complexes of common organic oxalic acid with atmospheric nucleation precursors, J.
650 Mol. Struct.: THEOCHEM, 951, 28-33, https://doi.org/10.1016/j.theochem.2010.04.004,
651 2010a.
652 Xu, Y., Nadykto, A. B., Yu, F., Herb, J., and Wang, W.: Interaction between common organic
653 acids and trace nucleation species in the Earth's atmosphere, J. Phys. Chem. A, 114, 387-96,
654 https://doi.org/10.1021/jp9068575, 2010b.
655 Xu, W., and Zhang, R.: Theoretical investigation of interaction of dicarboxylic acids with
656 common aerosol nucleation precursors, J. Phys. Chem., 116, 4539-4550, https://doi.org/
657 10.1021/jp301964u, 2012.
658 Xu, W., and Zhang, R.: A theoretical study of hydrated molecular clusters of amines and
659 dicarboxylic acids, J. Chem. Phys., 139, 064312, https://doi.org/10.1063/1.4817497, 2013.
660 Xu, W., Gomez-Hernandez, M., Guo, S., Secrest, J., Marrero-Ortiz, W., Zhang, A. L., and Zhang,
661 R.: Acid-catalyzed reactions of epoxides for atmospheric nanoparticle growth, J. Am. Chem.
662 Soc., 136, 15477−15480, https://doi.org/10.1021/ja508989a, 2014.
663 Yao, L., Garmash, O., Bianchi, F., Zheng, J., Yan, C., Kontkanen, J., Junninen, H., Mazon, B. S.,
664 Ehn, M., Paasonen, P., Sipila, M., Wang, M., Wang, X., Xiao, S., Chen, H., Lu, Y., Zhang,

665 B., Wang, D., Fu, Q., Geng, F., Li, L., Wang, H., Qiao, L., Yang, X., Chen, J., Kerminen,
666 V., Petaja, T., Worsnop, D., Kulmala, M., Wang, L.: Atmospheric new particle formation
667 from sulfuric acid and amines in a Chinese megacity, Science, 361, 278-281,
668 https://doi.org/10.1126/science.aao4839, 2018.
669 Yu, H., McGraw, R., and Lee, S.-H.: Effects of amines on formation of sub-3 nm particles and
670 their subsequent growth, Geophys. Res. Lett., 39, L02807,
671 https://doi.org/10.1029/2011GL050099, 2012.
672 Yue, D. L., Hu, M., Zhang, R. Y., Wang, Z. B., Zheng, J., Wu, Z. J., Wiedensohler, A., He, L. Y.,
673 Huang, X. F., and Zhu, T.: The roles of sulfuric acid in new particle formation and growth in
674 the mega-city of Beijing, Atmos. Chem. Phys. 10, 4953–4960, https://doi.org/ 10.5194/acp-
675 10-4953-2010, 2010.
676 Yue, D. L., Hu, M., Zhang, R. Y., Wu, Z. J., Su, H., Wang, Z. B., and Wiedensohler, A.:
677 Potential contribution of new particle formation to cloud condensation nuclei in Beijing,
678 Atmos. Environ., 45, 6070-6077, https://doi.org/ 10.1016/j.atmosenv.2011.07.037, 2011.
679 Zhang, R., Suh, I., Zhao, J., Zhang, D., Fortner, E. C., Tie, X., Molina, L. T., and Molina, M. J.:
680 Atmospheric new particle formation enhanced by organic acids, Science, 304, 1487-1490,
681 https://doi.org/10.1126/science.1095139, 2004.
682 Zhang, R., Wang, L., Khalizov, A. F., Zhao, J., Zheng, J., McGraw, R. L., and Molina, L. T.:
683 Formation of nanoparticles of blue haze enhanced by anthropogenic pollution, Proc. Natl.
684 Acad. Sci. USA, 106, 17650-17654, https://doi.org/10.1073/pnas.0910125106, 2009.
685 Zhang, R.: Getting to the critical nucleus of aerosol formation, Science, 328, 1366-1367,
686 https://doi.org/10.1126/science.1189732, 2010.

687 Zhang, R., Khalizov, A.F., Wang, L., Hu, M., Xu, W.: Nucleation and growth of nanoparticles in
688 the atmosphere, Chem. Rev., 112, 1957-2011, https://doi.org/10.1021/cr2001756, 2012.
689 Zhang, R., Wang, G., Guo, S., Zamora, M. L., Ying, Q., Lin, Y., Wang, W., Hu, M., and Wang
690 Y.: Formation of urban fine particulate matter, Chem. Rev., 115, 3803-3855,
691 https://doi.org/10.1021/acs.chemrev.5b00067, 2015.
692 Zhang, H., Kupiainen-Määttä, O., Zhang, X., Molinero, V., Zhang, Y., and Li, Z., The
693 enhancement mechanism of glycolic acid on the formation of atmospheric sulfuric acid–
694 ammonia molecular clusters, J. Chem. Phys., 146, 184308,
695 https://doi.org/10.1063/1.4982929, 2017.
696 Zhao, J., Khalizov, A., Zhang, R., and McGraw, R.: Hydrogen bonding interaction of molecular
697 complexes and clusters of aerosol nucleation precursors, J. Phys. Chem. A 113, 680–689,
698 https://doi.org/10.1021/jp806693r, 2009.
699 Zhu, Y. P., Liu, Y. R., Huang, T., Jiang, S., Xu, K. M., Wen, H., Zhang, W. J., and Huang, W.:
700 Theoretical study of the hydration of atmospheric nucleation precursors with acetic acidJ,
701 Phys. Chem. A, 118, 7959-7974, https://doi.org/10.1021/jp506226z, 2014.
702

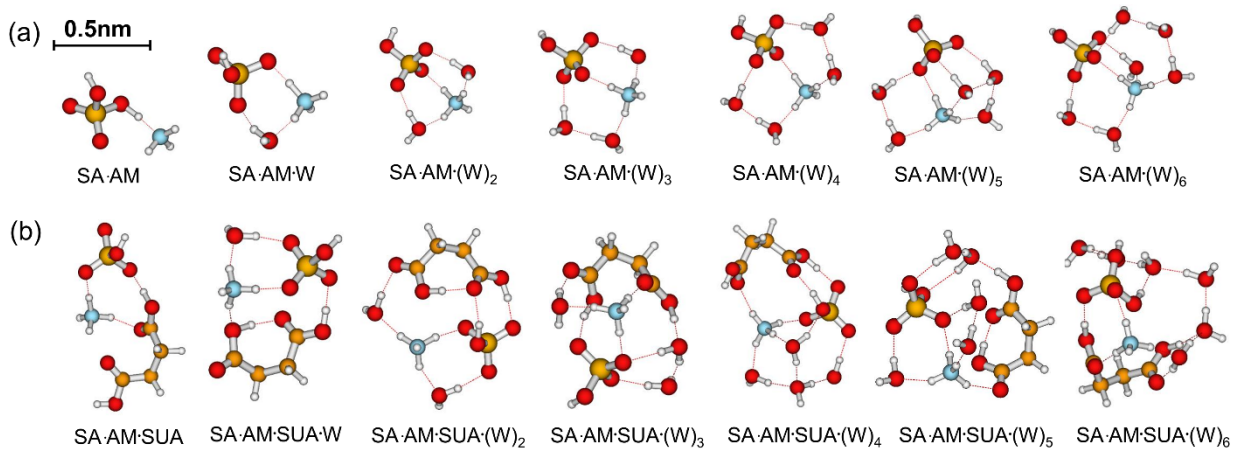

703

704 FIG. 1. Most stable configurations of the hydrated SA•AM clusters and the clusters with one

705 SUA addition. The hydration is with 0-6 water molecules. The sulfur (carbon) atoms are depicted

706 as large (small) yellow balls, oxygen atoms in red, nitrogen atoms in blue, and hydrogen atoms

707 in white. The dash line denotes the hydrogen bond.

708

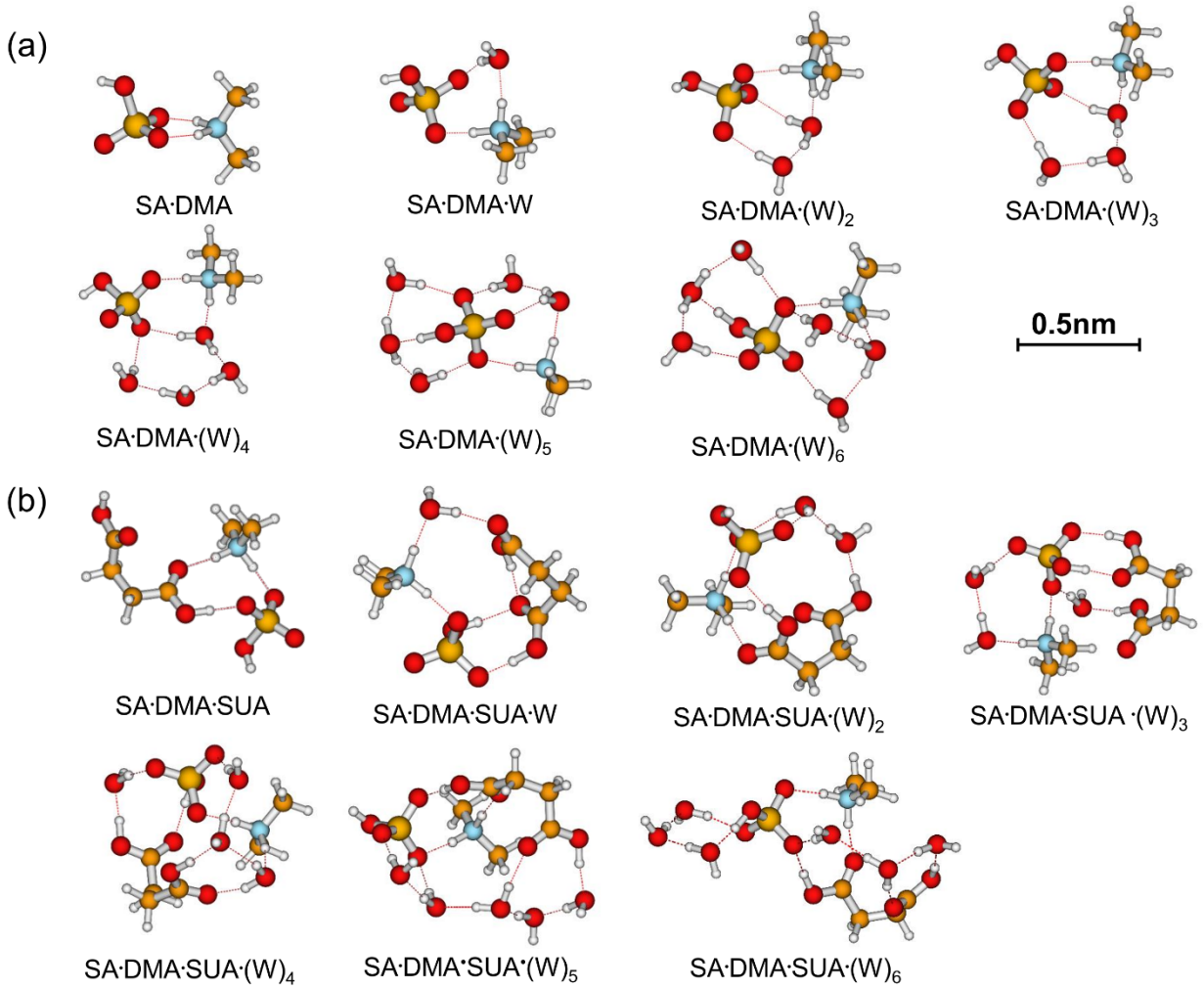

709

710 FIG. 2. Most stable configurations of the hydrated SA•DMA clusters and the clusters with one

711 SUA addition. The hydration is with 0-6 water molecules.

712

713

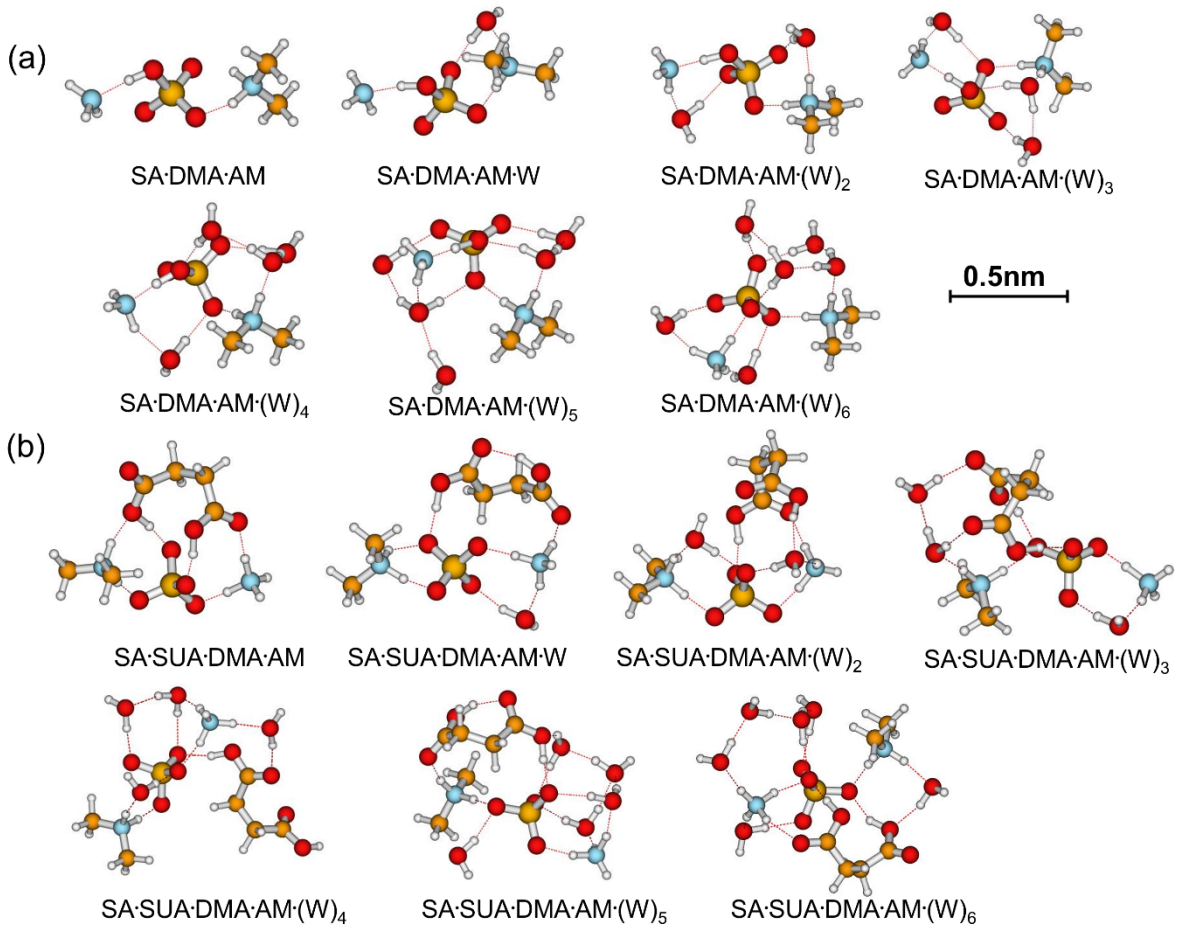

714

715 FIG. 3. Most stable configurations of the hydrated SA•DMA•AM clusters and the clusters with

716 one SUA addition. The hydration is with 0-6 water molecules.

717

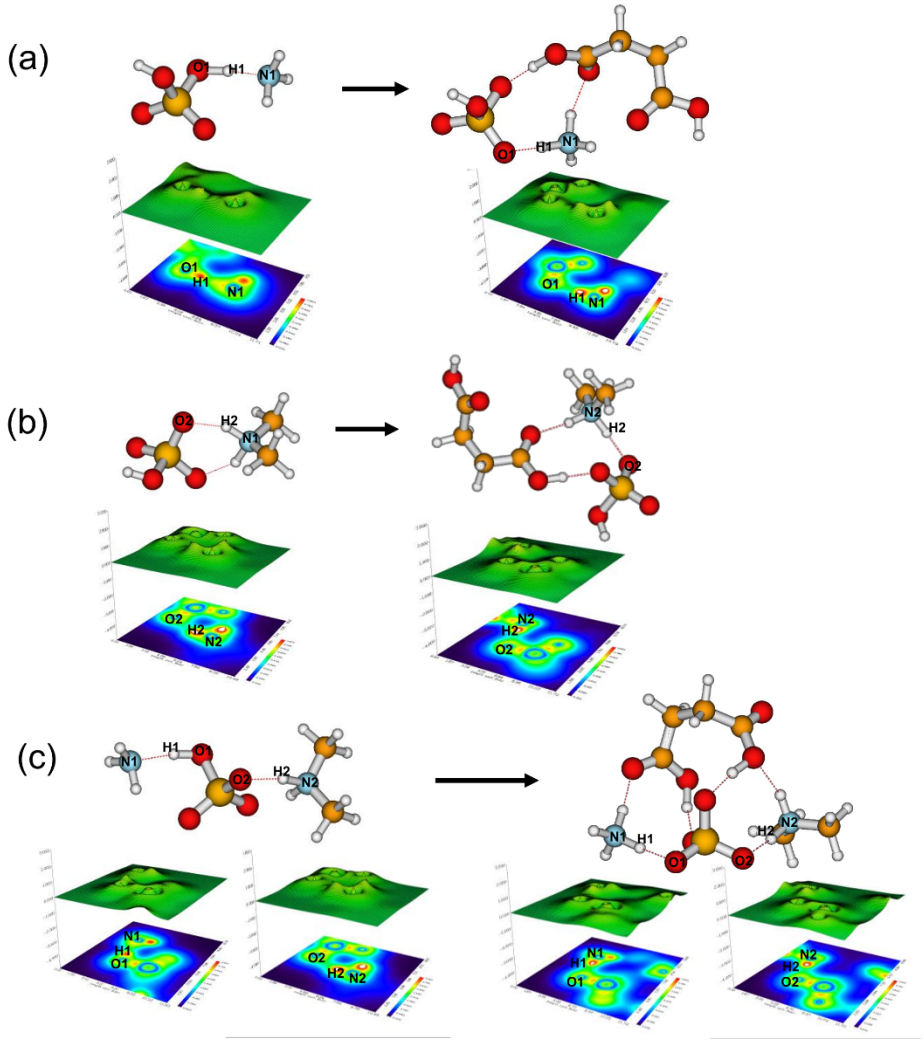

718

719 FIG. 4. Relief maps with the projection of localized orbital locator for clusters of (a) SA•AM and
720 SA•AM•SUA, (b) SA•DMA, SA•DMA•SUA, and (c) SA•DMA•AM and SA•DMA•AM•SUA.
721 Hydrogen bonds are shown as dashed lines. A large LOL value reflects that electrons are greatly
722 localized, indicating the existence of a covalent bond.

723

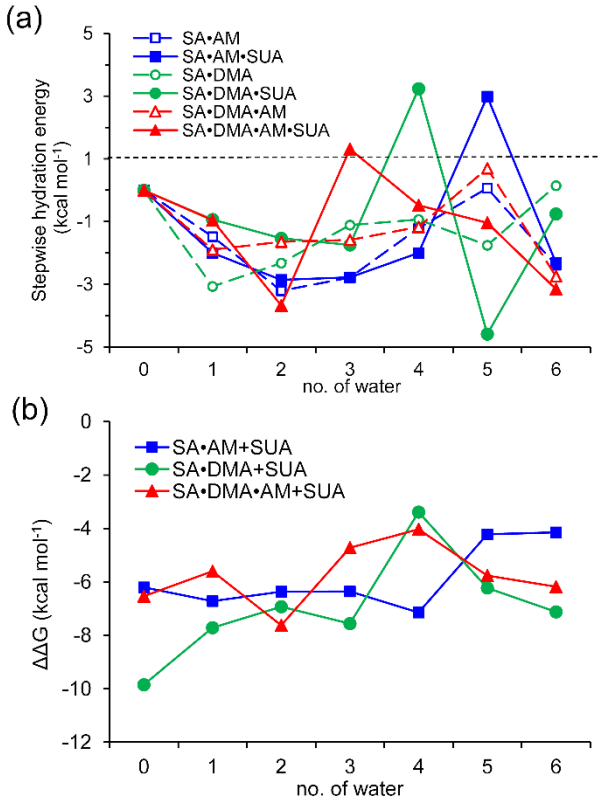

FIG. 5. Stepwise hydration free energies (a) and the relative Gibbs free energy changes due to addition of one SUA molecule to SA•base clusters (b) at T=298.15 K and p=1 atm. The free energy is calculated at the PW91PW91/6-311++G(2d, 2p) level.

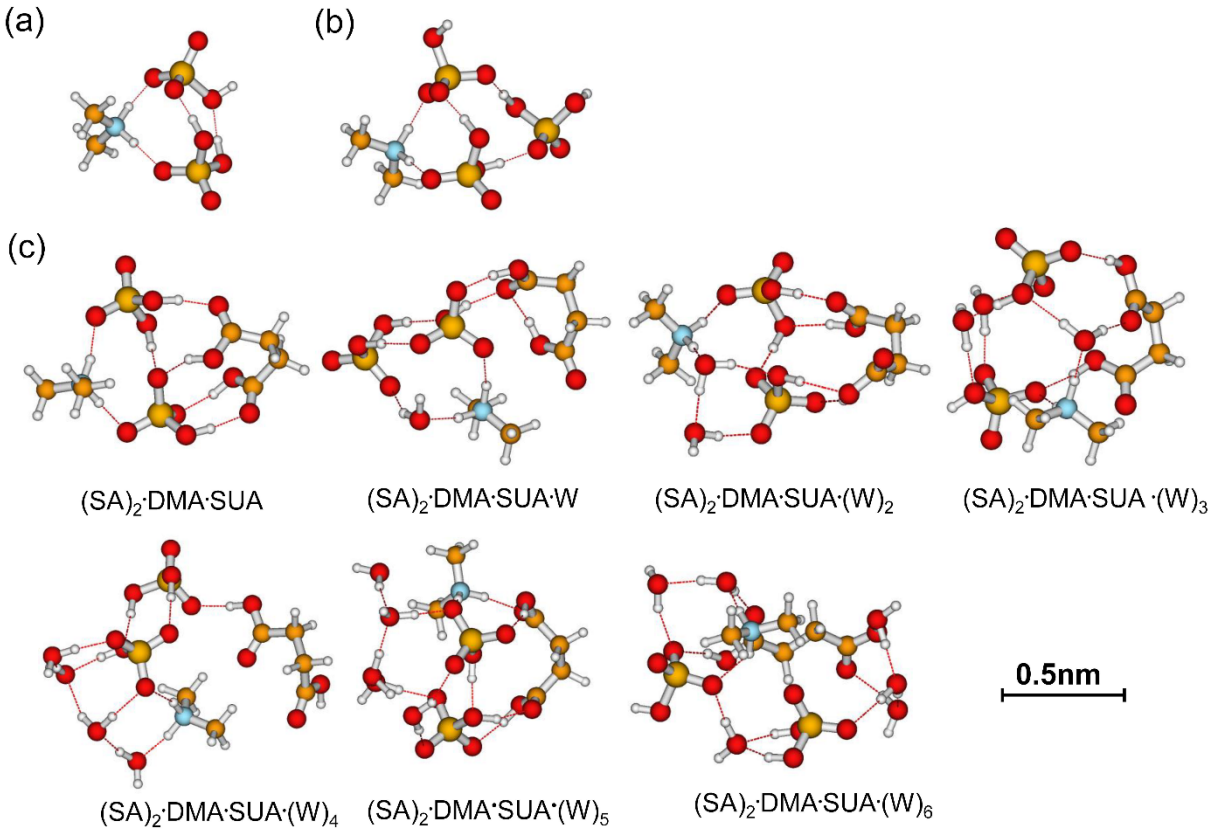

FIG. 6. Most stable configurations of (a) unhydrated $(SA)_2$•DMA, (b) $(SA)_2$•DMA, and (c) the hydrated $(SA)_2$•DMA•SUA clusters. The hydration is with 0-6 water molecules (W).

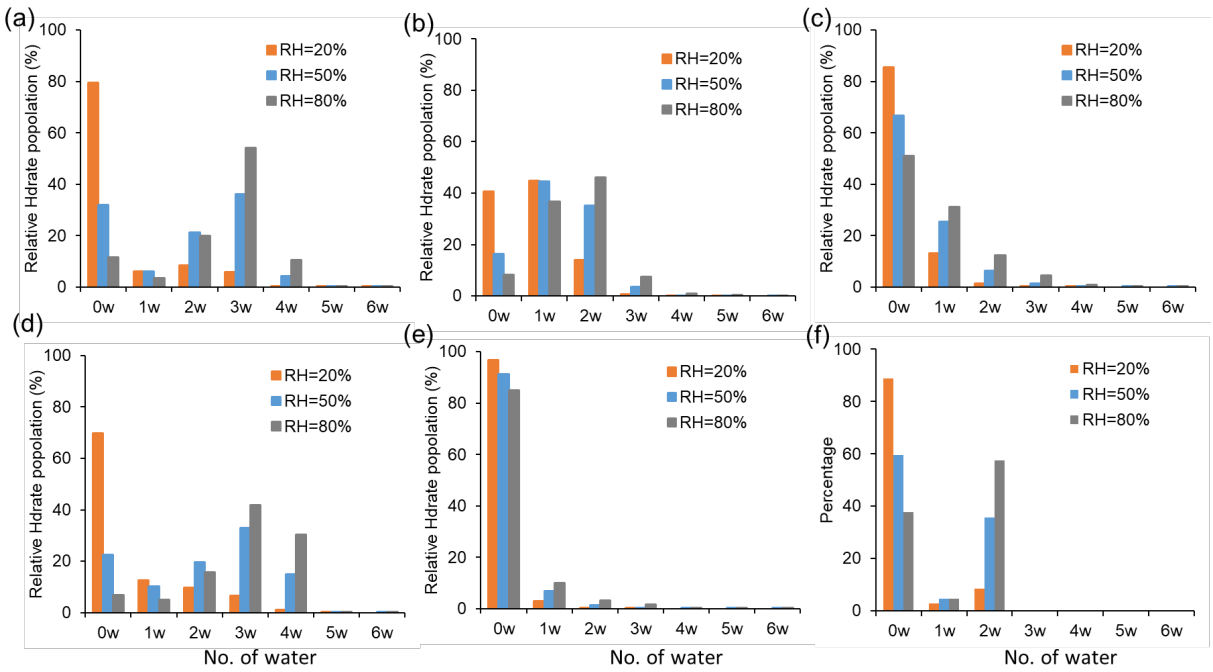

736

737 FIG. 7. Hydrate distributions of clusters under different RH levels (20%, 50% and 80%). (a), (b),

738 and (c) are clusters for SA•AM, SA•DMA, and SA•DMA•AM, respectively. (d), (e) and (f) are

739 clusters with one SUA addition on the basis of (a), (b) and (c) clusters. In all RH cases, T=298 K.

740

741

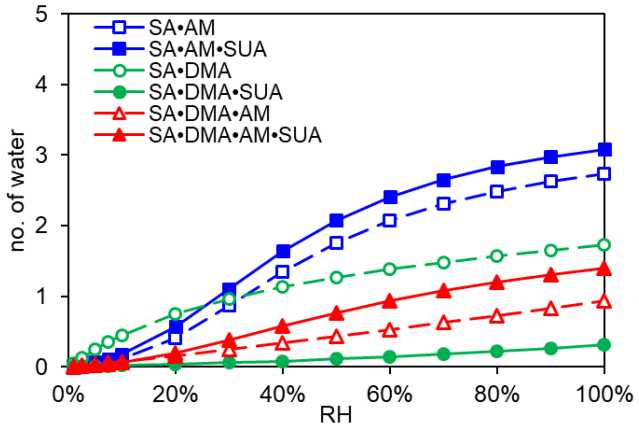

742 FIG. 8. Average hydration numbers per cluster for various SA•base clusters at 298.15 K.

743

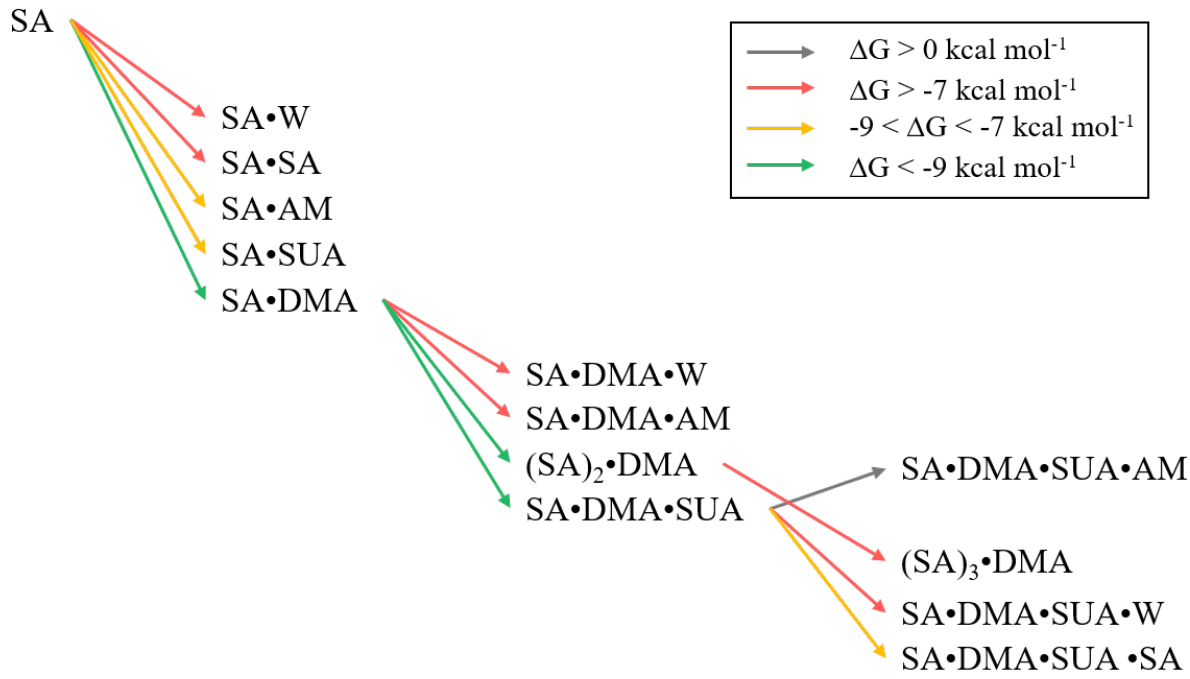

744

745 Fig. 9. Possible pathways for cluster formation based on free energies of formation.

746

747

748

749

750 Table 1. Theoretical and experimental values of the free energy change for several basic

751 reactions in kcal mol^{-1}.

Reactions	This study		refs
	PW91PW91/6-311++G(2df,2pd)	M06-2X/6-311++G(3df,3pd)	
SA+AM →SA•AM	-7.65	-8.00	-8.5[a,*], -7.77[b], -6.64[c], -7.84[d]
SA+DMA→SA•DMA	-11.13	-11.24	13.66[c], 11.38[e]
SA•AM+W→SA•AM•W	-1.48	-0.07	-1.41[b], -1.67[f]
SA•DMA+W→SA•DMA•W	-3.06	-3.63	-3.67[e], -2.89[f]
SA•AM+SUA→SA•AM•SUA	-6.20	-7.29	-
SA•DMA+SUA →SA•DMA•SUA	-9.86	-11.46	-

752 [a] From Hanson and Eisele (2002)

753 [b] From Nadykto and Yu (2007)

754 [c] From Kurtén et al. (2008)

755 [d] From Elm et al. (2012)

756 [e] From Nadykto et al. (2011)

757 [f] From Henschel et al. (2014)

758 [*] corresponds to experimental results.

759

760 Table 2. Calculated binding energy ΔE(ZPE), enthalpy ΔH, and Gibbs free energy ΔG (at

761 T=298.15 K and p=1 atm) at the PW91PW91/6-311++G(2d, 2p) level of theory for the hydrated

762 clusters. Energies are in kcal mol^{-1}.

Reactions	*ΔE(ZPE)*	*ΔH*	*ΔG*
SA+AM → SA•AM	-15.95	-16.51	-7.65
SA+AM+W → SA•AM•W	-26.40	-28.02	-9.13
SA+AM+2W → SA•AM•$(W)_2$	-39.14	-41.58	-12.33
SA+AM+3W → SA•AM•$(W)_3$	-49.96	-52.98	-15.11
SA+AM+4W → SA•AM•$(W)_4$	-59.63	-63.30	-16.32
SA+AM+5W → SA•AM•$(W)_5$	-69.20	-73.58	-16.26
SA+AM+6W → SA•AM•$(W)_6$	-78.71	-83.37	-18.64
SA+DMA → SA•DMA	-21.16	-21.11	-11.13
SA+DMA+W →SA• DMA•W	-33.46	-34.13	-14.19
SA+DMA+2W → SA•DMA•$(W)_2$	-45.02	-46.60	-16.51
SA+DMA+3W → SA•DMA•$(W)_3$	-54.37	-56.57	-17.62
SA+DMA+4W → SA•DMA•$(W)_4$	-62.47	-65.25	-18.56
SA+DMA+5W → SA•DMA•$(W)_5$	-75.68	-79.92	-20.31
SA+DMA+6W → SA•DMA•$(W)_6$	-84.43	-89.24	-20.16
SA+SUA+AM → SA•SUA•AM	-34.19	-34.69	-13.85
SA+SUA+AM+W → SA•SUA•AM•W	-45.65	-47.18	-15.85
SA+SUA+AM+2W → SA•SUA•AM•$(W)_2$	-58.95	-61.44	-18.70
SA+SUA+AM+3W → SA•SUA•AM•$(W)_3$	-70.41	-73.52	-21.47
SA+SUA+AM+4W → SA•SUA•AM•$(W)_4$	-80.92	-84.95	-23.47
SA+SUA+AM+5W → SA•SUA•AM•$(W)_5$	-86.75	-90.96	-20.48
SA+SUA+AM+6W → SA•SUA•AM•$(W)_6$	-98.52	-104.27	-22.80
SA+SUA+DMA → SA•SUA•DMA	-42.01	-41.42	-20.98
SA+SUA+DMA+W → SA•SUA•DMA•W	-54.80	-55.47	-21.92
SA+SUA+DMA+2W → SA•SUA•DMA•$(W)_2$	-64.86	-66.03	-23.45
SA+SUA+DMA+3W → SA•SUA•DMA•$(W)_3$	-75.90	-78.21	-25.19
SA+SUA+DMA+4W → SA•SUA•DMA•$(W)_4$	-82.83	-86.21	-21.95
SA+SUA+DMA+5W → SA•SUA•DMA•$(W)_5$	-92.80	-96.19	-26.54
SA+SUA+DMA+6W → SA•SUA•DMA•$(W)_6$	-103.04	-107.49	-27.29
2SA+SUA+DMA → $(SA)_2$•SUA•DMA	-62.90	-63.35	-26.12
2SA+SUA+DMA+W → $(SA)_2$•SUA•DMA•W	-69.95	-70.90	-25.11
2SA+SUA+DMA+2W → $(SA)_2$•SUA•DMA•$(W)_2$	-79.07	-80.72	-25.30
2SA+SUA+DMA+3W → $(SA)_2$•SUA•DMA•$(W)_3$	-91.67	-94.06	-28.71
2SA+SUA+DMA+4W → $(SA)_2$•SUA•DMA•$(W)_4$	-93.90	-96.57	-24.36
2SA+SUA+DMA+5W → $(SA)_2$•SUA•DMA•$(W)_5$	-115.58	-120.45	-31.69

$2SA+SUA+DMA+6W \rightarrow (SA)_2 \bullet SUA \bullet DMA \bullet (W)_6$	-108.55	-112.07	-22.50
$SA+DMA+AM \rightarrow SA \bullet DMA \bullet AM$	-23.83	-33.01	-14.15
$SA+DMA+AM+W \rightarrow SA \bullet DMA \bullet AM \bullet W$	-44.15	-45.58	-16.05
$SA+DMA+AM+2W \rightarrow SA \bullet DMA \bullet AM \bullet (W)_2$	-54.34	-56.54	-17.69
$SA+DMA+AM+3W \rightarrow SA \bullet DMA \bullet AM \bullet (W)_3$	-66.01	-69.12	-19.27
$SA+DMA+AM+4W \rightarrow SA \bullet DMA \bullet AM \bullet (W)_4$	-75.88	-79.62	-20.44
$SA+DMA+AM+5W \rightarrow SA \bullet DMA \bullet AM \bullet (W)_5$	-83.63	-87.99	-19.74
$SA+DMA+AM+6W \rightarrow SA \bullet DMA \bullet AM \bullet (W)_6$	-97.07	-102.91	-22.48
$SA+SUA+DMA+AM \rightarrow SA \bullet SUA \bullet DMA \bullet AM$	-54.69	-56.03	-20.69
$SA+SUA+DMA+AM+W \rightarrow SA \bullet SUA \bullet DMA \bullet AM \bullet W$	-62.07	-63.89	-21.65
$SA+SUA+DMA+AM+2W \rightarrow SA \bullet SUA \bullet DMA \bullet AM \bullet (W)_2$	-77.31	-80.08	-25.32
$SA+SUA+DMA+AM+3W \rightarrow SA \bullet SUA \bullet DMA \bullet AM \bullet (W)_3$	-83.64	-87.00	-24.00
$SA+SUA+DMA+AM+4W \rightarrow SA \bullet SUA \bullet DMA \bullet AM \bullet (W)_4$	-92.14	-95.95	-24.48
$SA+SUA+DMA+AM+5W \rightarrow SA \bullet SUA \bullet DMA \bullet AM \bullet (W)_5$	-104.97	-110.11	-25.51
$SA+SUA+DMA+AM+6W \rightarrow SA \bullet SUA \bullet DMA \bullet AM \bullet (W)_6$	-115.86	-121.79	-28.66

763
764

765 Table 3. Typical ranges of gas-phase concentrations (molecules cm^{-3}) for sulfuric acid,

766 ammonium, dimethylamine, and succinic acid in the atmosphere.

Precursors	Sulfuric acid [a]	Ammonium[b]	Dimethylamine[c]	Succinic acid[d]
number concentration	$1x10^5$~$1x10^7$	$1x10^9$~$1x10^{11}$	$1x10^7$~$1x10^9$	$1x10^8$~$1x10^9$

767 [a] Zhang et al. (2012).

768 [b] Seinfeld and Pandis (1998).

769 [c] Ge et al. (2011).

770 [d] Ho et al. (2007).

771

772 Table 4. Number of Proton Transfers within hydrated Clusters (T = 298.15 K).

Cluster	No. of water						
	0	*1*	*2*	*3*	*4*	*5*	*6*
SA[a]	0	0	0	1	1	1	1
SA•AM	0	1	1	1	1	1	1
SA•AM•SUA	1	1	1	1	1	1	1
SA•DMA	1	1	1	1	1	1	1
SA•DMA•SUA	1	1	1	1	1	1	1
SA•DMA•AM	1	1	1	1	1	1	2
SA•DMA•AM•SUA	2	2	2	2	2	2	2

773 [a] From Xu and Zhang (2013)

774

775 Table 5. Laplacian bond order (LBO) of the newly formed covalent bond (nitrogen-hydrogen
776 bond) between in the clusters (a.u.).

Clusters	Bonds	No. of water						
		0	*1*	*2*	*3*	*4*	*5*	*6*
SA•AM	N1-H1	-	0.383	0.577	0.586	0.580	0.636	0.663
SA•AM•SUA	N1-H1	0.464	0.575	0.586	0.621	0.609	0.663	0.607
SA•DMA	N2-H2	0.542	0.503	0.571	0.571	0.577	0.579	0.610
SA•DMA•SUA	N2-H2	0.551	0.548	0.598	0.613	0.583	0.613	0.581
SA•DMA•AM	N1-H1	-	-	-	-	-	-	0.525
	N2-H2	0.489	0.483	0.608	0.553	0.533	0.591	0.567
SA•DMA•AM•SUA	N1-H1	0.420	0.521	0.483	0.321	0.607	0.591	0.677
	N2-H2	0.498	0.411	0.518	0.611	0.501	0.564	0.568

777 Note: N1 is the nitrogen atom on the ammonia (AM) molecule; N2 is the nitrogen atom on the
778 dimethylamine (DMA) molecule; H1 is the hydrogen atom on one of the hydroxyl functions of sulfuric
779 acid (SA) molecule and bound to N1; H2 is the hydrogen atom on one of the hydroxyl functions of SA
780 (SA) molecule and bound to N2.

781

Table 6. Gibbs free energy (ΔG, kcal mol^{-1}), interaction energy (ΔH^0, kcal mol^{-1}), and cluster concentration at equilibrium for basic clustering reactions. The right-hand side of clustering reactions is the product clusters in eq. 9, and the core clusters and addition molecules in eq. 9 are listed here as well.

Cluster reactions	ΔG	ΔH^0	Dipole Moment (Debye)	Cluster		
				Core cluster	Molecule for addition	[Cluster] (cm^{-3})
SA+SA ↔ $(SA)_2$	-3.72	-13.08	0.0008	SA	SA	10^{-7}~10^{-3}
SA+SUA ↔ SA•SUA	-8.61	-17.94	4.2631	SA	SUA	10^{0}~10^{3}
SA+AM ↔ SA•AM	-6.36	-14.38	6.5915	SA	AM	10^{-1}~10^{-3}
SA+DMA ↔ SA•DMA	-11.41	-18.38	8.2081	SA	DMA	10^{1}~10^{5}
SA•SUA+SA ↔ $(SA)_2$•SUA	-1.02	-11.04	4.6588	SA•SUA	SA	10^{-14}~10^{-9}
SA•AM+SA ↔ $(SA)_2$•AM	-9.46	-19.53	7.4060	SA•AM	SA	10^{-9}~10^{-3}
SA•AM+SUA ↔ SA•AM•SUA	-6.20	-16.01	8.7764	SA•AM	SUA	10^{-8}~10^{-3}
SA•DMA+SA ↔ $(SA)_2$•DMA	-10.53	-21.16	7.0470	SA•DMA	SA	10^{-6}~10^{0}
SA•DMA+SUA ↔ SA•DMA•SUA	-9.86	-19.07	7.4559	SA•DMA	SUA	10^{-3}~10^{2}
$(SA)_2$•DMA+SA ↔ $(SA)_3$•DMA	-6.10	-15.25	7.4060	$(SA)_2$•DMA	SA	10^{-16}~10^{-8}
SA•DMA•SUA+SA ↔ $(SA)_2$•DMA•SUA	-5.13	-19.07	5.2795	SA•DMA•SUA	SA	10^{-14}~10^{-7}

785 Table 7. Concentration Ratios between SUA•SA•X and $(SA)_2$•X Clusters, with X = W, AM, and

786 DMA.

SUA/SA	X=(None)	X=W	X=AM	X=DMA
10:1	3.80E+04	5.30E+03	4.11E-02	3.19E+00
100:1	3.80E+05	5.30E+04	4.11E-01	3.19E+01
1000:1	3.80E+06	5.30E+05	4.11E+00	3.19E+02
10 000:1	3.80E+07	5.30E+06	4.11E+01	3.19E+03

787